Bending elasticity of the surfactant monolayer in droplet microemulsions: Determination by a combination of dynamic light scattering and neutron spin-echo spectroscopy

Thomas Hellweg* and Dominique Langevin†
Centre de Recherche Paul Pascal, CNRS Avenue Albert Schweitzer, 33600 Pessac, France
(Received 2 June 1997; revised manuscript received 9 February 1998)

The bending elastic energy of a surfactant monolayer at the oil-water interface in a microemulsion system can be described by the spontaneous monolayer curvature and two elastic constants κ and $\bar{\kappa}$. Here we present the determination of these constants by a combination of dynamic light scattering and neutron spin-echo spectroscopy for the octane$-C_{10}E_5$-water microemulsion on the water continuous side of the phase diagram. Small-angle neutron scattering data are also presented and compared to the light scattering results. [S1063-651X(98)01006-X]

PACS number(s): 68.10.−m, 78.70.+Nx, 66.10.Cb, 78.35.+c

I. INTRODUCTION

Microemulsions are thermodynamically stable mixtures of oil and water, stabilized by surfactants and in some cases additionally by cosurfactants [1,2]. The microstructures formed in these systems are frequently droplets, either of oil or water, covered by a surfactant monolayer, dispersed in the continuous phase. In mixtures containing comparable amounts of oil and water, bicontinuous structures may also occur [3]. The stability of these different phases is mainly determined by the elastic properties of the amphiphilic monolayer [4].

In the case of droplet microemulsions the theory of curvature elasticity has been used for the description of the shape fluctuation of the drops [5,6]. More generally, the knowledge of the elastic constants is necessary for an understanding of the properties of microemulsions [7,8] and their determination, which is not an easy task, has been focused using a wide range of different experimental methods [9–14]. In recent years nonionic surfactants of the type alkyloligoglycolether (C_nE_j) have been used in studies of microemulsions because they form ternary microemulsions and no additional cosurfactant has to be added [15,16]. Another important feature of these systems is that the microstructure can be easily changed just by choosing the appropriate temperature if the phase behavior is known [15,16]. The elastic constants κ and $\bar{\kappa}$ are in principle directly accessible by neutron spin-echo spectroscopy (NSES) [17–19]. In practice, it is difficult to extract them from the correlation functions for the droplet motions obtained by NSES because of the small number of data points that are measured and the rather bad data statistics. Due to these facts it is necessary to combine the information from NSES with data obtained from other sources. To our knowledge up to now the data analysis has been done using a combined fit of NSES and small-angle neutron scattering (SANS) data [17–19]. In our study we present a combination of NSES with dynamic light scattering (DLS), which allows for a direct determination of the relaxation times of the deformation modes of the microemulsion droplets. Also SANS data obtained for the same sample composition will be discussed. The determination of the sum $2\kappa+\bar{\kappa}$ from the polydispersity index computed analyzing SANS data is a well-known procedure [14]. In our study we will describe the possibility to determine this sum from DLS data.

II. THEORY

A. Microemulsion theory

The well-defined microstructures in microemulsions are formed because the surfactant layer has a preferred curvature C_0. A positive value of C_0 indicates a curving tendency towards water and a negative value a curving tendency towards oil. The droplet radius for a given system can be predicted by

$$R=\frac{3\phi}{[S]\Sigma}, \tag{1}$$

where $[S]$ is the surfactant concentration, ϕ the dispersed phase volume fraction, and Σ the area in the monolayer occupied by a surfactant molecule [2]. The area occupied per surfactant molecule is relatively constant and the monolayer can be regarded as approximately incompressible [1]. Under the conditions of microemulsion formation, one important contribution to the free energy of the systems is the curvature energy of the surfactant layer. The curvature energy can be described by the Helfrich equation [4]

$$F=\frac{1}{2}\kappa(C_1+C_2-2C_0)^2+\bar{\kappa}C_1C_2. \tag{2}$$

Here κ and $\bar{\kappa}$ are the mean (splay) and the Gaussian (saddle-splay) bending elastic constant. C_1 and C_2 are the principal curvatures of the surfactant film. In the case of droplet microemulsions $C_1=C_2=1/R$.

*Present address: Dr. T. Hellweg, Institut für Physik, Materialforschung und Flüssigkeiten, TU-Chemnitz, D-09107 Chemnitz, Federal Republic of Germany.
†Author to whom correspondence should be addressed.

The knowledge of the bending elastic constants can be achieved by using experimental methods, which are able to resolve fluctuations of the oil-water interface. For droplet microemulsions it is possible to describe these fluctuations in terms of spherical harmonics [5,20,21]. This offers the possibility to calculate a dynamic structure factor $S(q,\omega)$ or its Fourier transform $S(q,t)$, which can be used to analyze dynamical measurements by neutron spin-echo spectroscopy [17]. For the scattering from thin shells $S(q,t)$ has been derived [5] and has the form

$$S(q,t)=\langle \rho_q(t)\rho_{-q}(0)\rangle \exp(-D_0 q^2 t) \times\left[4\pi[j_0(qR)]^2+\sum f_l(qR)\langle u_l(0)u_l(t)\rangle\right]. \tag{3}$$

Therefore, the time correlation function takes the form [19]

$$I(q,t)=\left\langle \exp(-\Gamma_1 t)V_s^2(\Delta\rho)^2\left[f_0(qR)+\sum_{l\geqslant 2}\frac{2l+1}{4\pi}f_l(qR)\langle|u_l|^2\rangle\exp(-\Gamma_l t)\right]\right\rangle_R, \tag{4}$$

which is a sum of at least two exponential decays if terms corresponding to $l>2$ are omitted. The first contribution represents the translational motion of the particles and the second represents the shape fluctuations of the particles. Γ_l is the relaxation rate of the corresponding mode.

For the relaxation time τ_2 of the modes corresponding to the second-order spherical harmonic ($l=2$) the expression

$$\tau_2^{-1}=\frac{1}{\eta R^3}\left[4\kappa-\overline{\kappa}-\frac{kT(\ln\phi-1)}{4\pi}\right]\frac{1}{Z(2)} \tag{5}$$

was derived [21] at the emulsification failure boundary, where the microemulsion droplets are swollen to their maximum size. $Z(l)$ is given by

$$Z(l)=\frac{(2l+1)(2l^2+2l-1)}{l(l+1)(l+2)(l-1)}, \tag{6}$$

which leads for $l=2$ to 55/24. In these expressions, the oil and water viscosities were assumed to be equal. In practice, they are somewhat different and a more rigorous equation can be used [22]

$$Z(l)=\frac{[(2l^2+4l+3)E+2l(l+2)][2(l^2-1)E+2l^2+1]}{(l-1)l(l+1)(l+2)(2l+1)(E+1)}. \tag{7}$$

Here E is the ratio of the viscosities of the interior and the continuous phase of the droplets. In the limit of equal viscosities and for $l=2$ Eq. (7) leads to a ratio of 52.5/24. The difference compared to Eq. (6) is of minor importance and probably due to different approximations in the hydrodynamic calculations.

This theoretical description in terms of spherical harmonics also allows one to relate the size polydispersity index p of the microemulsion droplets and the bending elastic constants [5]

$$p^2=\frac{kT}{8\pi(2\kappa+\overline{\kappa})+2kT(\ln\phi-1)}. \tag{8}$$

The quantity p is accessible by neutron scattering [14] or light scattering experiments.

B. NSE spectroscopy

In a neutron spin-echo spectrometer, polarized neutrons are flying in a first set of coils thereby undergoing Larmor precession. Then they are scattered by a sample, inverted in spin, and passed through a second set of coils. The scattering process leads thereby to a change in the speed of the neutrons and thus a difference in the number of precessions before and after the sample if the magnetic fields on both sides of the sample are exactly identical to each other. The angle $\Delta\psi$ between the spin of the incident neutrons and the neutrons finally reaching the detector is analyzed using the scattered intensity

$$P_s=P_0\cos(\Delta\psi). \tag{9}$$

Here P_0 is the detected intensity if no sample is present. The probability for a scattering process with an energy transfer ω is described by the dynamic structure factor $S(q,\omega)$. Averaging $\cos(\Delta\psi)$ with $S(q,\omega)$ leads to

$$P_s=\langle\cos(\Delta\psi)\rangle=\frac{\int S(q,\omega)\cos(t\Delta\omega)d\omega}{\int S(q,\omega)d\omega}, \tag{10}$$

with $\Delta\psi=t\Delta\omega$. This Fourier transform in time can be rewritten as

$$P_s(q,t)=\frac{I(q,t)}{I(q,0)}. \tag{11}$$

The Fourier time is given by

$$t=\frac{\gamma l_0 H_0 m^2}{2\pi h^2}\lambda^3. \tag{12}$$

Here λ is the wavelength of the neutrons, γ the gyromagnetic ratio, and l_0H_0 the integral of the magnetic field along the neutron's path [23]. For a wavelength of 0.6 nm, a time window of 18 ns can be probed, which is appropriate for the droplets motions expected in microemulsions. As a result one obtains directly the normalized intensity correlation function, which should correspond to the form given in Eq. (4).

Unfortunately the number of points obtained as a representation of this function is in most cases too small and the statistics of the individual points is too bad to allow for a multiexponential fit or for an analysis using the Laplace transformation and maximum entropy methods [24]. Without additional information it is only possible to extract an effective diffusion coefficient from the data by using a first- or second-order cumulant analysis [25]. In the previous studies

of microemulsions using NSES [17,19] the q variations of the effective diffusion coefficients are fitted by expressions of the type

$$\Gamma_{eff}=A(q)Dq^2+\sum_{l\geqslant 2} B_l(q)\langle|u_l|^2\rangle\Gamma_l, \tag{13}$$

which are obtained by calculating the first cumulant of the correlation function [Eq. (4)]. The translational diffusion coefficient D in this expression is usually calculated using the droplet radius derived from SANS experiments [17–19]. This radius is smaller than the hydrodynamic radius and the diffusional contribution to the decay is therefore slightly overestimated by this approach.

All modes corresponding to values of $l>2$ do not contribute significantly to the second term in Eq. (13) at moderate values of q ($qR\leqslant 10$) and are normally omitted. For the value of Γ_{eff} an apparent proportionality on q^3 is predicted [5]. This is analogous to the observations for Rouse-Zimm dynamics of polymers [26].

In our study we propose an alternative approach to analyze the data. Under the assumption that only the mode corresponding to $l=2$ contributes remarkably to the decay, the correlation functions from the NSES experiment will be fitted directly using a double exponential function of the form

$$\frac{I(q,t)}{I(q,0)}=a\exp(-D_0q^2t)+(1-a)\exp(-\Gamma t), \tag{14}$$

with

$$\tau_2^{-1}=\Gamma-D_0q^2 \tag{15}$$

for the relaxation time of the mode $l=2$. Therefore, $I(q,t)/I(q,0)$ contains only two adjustable parameters. The diffusion coefficient D_0 used here can be obtained from dynamic light scattering experiments. According to Eq. (4), the amplitudes a and $1-a$ should be proportional to

$$a\sim\frac{f_0(qR)}{f_0(qR)+\frac{5}{4\pi}f_2(qR)\langle|u_2|^2\rangle} \tag{16}$$

and

$$(1-a)\sim\frac{\frac{5}{4\pi}f_2(qR)\langle|u_2|^2\rangle}{f_0(qR)+\frac{5}{4\pi}f_2(qR)\langle|u_2|^2\rangle}. \tag{17}$$

τ_2 should be independent of the scattering angle, as in the case of Rouse-Zimm dynamics. In reality a slight q dependence may be observable because of the increasing contribution of modes corresponding to $l>2$ with increasing q, which cannot be resolved from the experimental data.

C. Dynamic light scattering

The intensity I of the light scattered from a dilute macromolecular or supramolecular solution is a fluctuating quantity due to the Brownian motion of the scattering particles. These fluctuations can be analyzed in terms of the normalized autocorrelation function $g^1(\tau)$ of the scattered electrical field E_s, which contains information about the structure and the dynamics of the scattering particles [27]

$$g^1(\tau)=\frac{\langle E_s^*(t)E_s(t+\tau)\rangle}{\langle I\rangle}. \tag{18}$$

Here E_s^* is the complex conjugate of E_s. Experimentally, the intensity correlation function $g^2(\tau)$ is determined

$$g^2(\tau)=\frac{\langle E_s^*(t)E_s(t)E_s^*(t+\tau)E_s(t+\tau)\rangle}{\langle I^2\rangle}, \tag{19}$$

which is related to $g^1(\tau)$ by the Siegert relation [27]

$$g^2(\tau)=1+C|g^1(\tau)|^2. \tag{20}$$

C is a coherence factor and depends on the experimental conditions. For an ideal solution of monodisperse particles the function $g^1(\tau)$ is represented by a single exponential

$$g^1(\tau)=\exp(-\Gamma\tau). \tag{21}$$

The relaxation rate Γ is connected with the translational diffusion coefficient D according to

$$\Gamma=Dq^2, \tag{22}$$

with the scattering vector $q=(4\pi n_0/\lambda)\sin(\theta/2)$. The scattering vector q depends on the wavelength λ of the incident light and the scattering angle θ.

For polydisperse samples the function $g^1(\tau)$ is given by a weighted sum of exponentials

$$g^1(\tau)=\int_0^\infty G(\Gamma)\exp(-\Gamma\tau)d\Gamma. \tag{23}$$

The function $g^1(\tau)$ can be analyzed by the method of cumulants [25] or by an inverse Laplace transformation. These methods provide the mean relaxation rate $\overline{\Gamma}$ of the distribution function $G(\Gamma)$ (z average). For the second analysis procedure mentioned above, the FORTRAN program CONTIN is available [28,29]. It is sometimes difficult to avoid the presence of spurious amounts of dust particles or high-molecular-weight impurities that give small contributions to the long-time tail of the experimental correlation functions. With CONTIN it is possible to distinguish these artifacts from the relevant relaxation mode contributing to $g^1(\tau)$.

The analysis of the light scattering data using CONTIN also allows for a determination of the size polydispersity of the microemulsion droplets because all the moments $\mu_n=\int_{\Gamma_{min}}^{\Gamma_{max}}G(\Gamma)\Gamma^n d\Gamma$ that describe the distribution function $G(\Gamma)$ are computed (for details see Ref. [29]). The polydispersity index is obtained from

$$p^2=\frac{\frac{\mu_2}{\mu_0}-\left(\frac{\mu_1}{\mu_0}\right)^2}{\left(\frac{\mu_1}{\mu_0}\right)^2}. \tag{24}$$

Using Eq. (22), from the mean relaxation rate $\bar{\Gamma}$ the average apparent translational diffusion coefficient D can be calculated. The measured apparent diffusion coefficient D depends on the concentration $[C]$ of the scattering particles. When $[C]$ is not too large ($\phi \leqslant 0.1$), one has

$$D = D_0(1 + k_D[C]), \tag{25}$$

where the diffusional virial coefficient k_D includes thermodynamic and frictional effects on D. If the interactions between the particles are negligible k_D becomes zero and D is equal to D_0. For dilute microemulsions (small $[C]$) stabilized by uncharged surfactants D is also close to D_0 [14,30,31]. Knowing the value of D_0, the hydrodynamic radius of the scattering particles R_H can be calculated by the Stokes-Einstein equation

$$D_0 = \frac{kT}{6\pi\eta R_H}, \tag{26}$$

with η the viscosity of the solvent (the continuous phase in the case of microemulsions).

D. Small-angle neutron scattering

For polydisperse shells as investigated in our study, one can account for polydispersity in the data analysis procedure by using an appropriate form factor [13,14,16]. We have chosen the form factor

$$F(q) = 16\pi^2(\Delta\rho)^2(\delta^2/q^2) \times \exp(-q^2t^2)[f_1(q) + f_2(q) + f_3(q) + f_4(q)], \tag{27}$$

with

$$f_1(q) = \frac{1}{2}q^2t^4[1 + \cos(2qR_0)\exp(-2\sigma^2q^2)],$$

$$f_2(q) = qt^2[R_0\sin(2qR_0) + 2q\sigma^2\cos(2qR_0)]\exp(-2\sigma^2q^2),$$

$$f_3(q) = \frac{1}{2}R_0^2[1 - \cos(2qR_0)\exp(-2\sigma^2q^2)],$$

$$f_4(q) = \frac{1}{2}\sigma^2[1 + 4qR_0\sin(2qR_0)\exp(-2\sigma^2q^2) + \cos(2qR_0)(4\sigma^2q^2 - 1)\exp(-2\sigma^2q^2)].$$

Here t is a thickness parameter and σ contains the information about the size polydispersity of the microemulsion drops. R_0 is the mean value of the shell inner and outer radii.

The absolute scattering intensity $I(q)$, which is the experimentally observed quantity is given by

$$I(q) = NF(q)S(q). \tag{28}$$

In this equation N is the number density of the scattering microemulsion droplets and $S(q)$ is the static structure factor. The strict validity of Eq. (28) is limited to the case of monodisperse spheres, but for the case of low polydispersities it can still be applied [32,33]. $S(q)$ describes the interactions between the droplets, which are generally well approximated by hard-sphere interactions in microemulsion systems based on nonionic surfactants. The influence of interparticle interactions as described by $S(q)$ can be estimated at least for $S(0)$ using the Carnahan-Starling expression [34,14,33]

$$S(0) = \frac{(1-\phi_{hs})^4}{(1-2\phi_{hs})^2 - \phi_{hs}^3(1-4\phi_{hs})}. \tag{29}$$

Here ϕ_{hs} is the hard-sphere volume fraction. ϕ_{hs} is about 14% larger in oil-in-water nonionic microemulsions than the dispersed volume fraction because of the water penetration in the surfactant layer [33]. However, $S(q)$ approaches unity for q values smaller than the minimum of $I(q)$. This was found even for fairly high volume fractions in nonionic surfactant systems (see, for example, Fig. 8 in Ref. [33]). Since the value of the radius is fixed by the position of the minimum of $I(q)$, the approximation of $S(q) \approx 1$ in Eq. (28) does not lead to a significant error in the determination of R_0 if the low-q data are omitted in the fitting procedure.

III. EXPERIMENT

A. Phase behavior

For studies of microemulsions it is essential to know the phase behavior of the system under investigation in the region of interest. The principal features for systems of the type water-C_nE_j-oil are always similar; only the positions of the phase boundaries with respect to the temperature differ with respect to the exact type of surfactant and oil employed [16]. In Fig. 1 the part of the phase diagram we recorded for C_8H_{18}-$C_{10}E_5$-water is shown. The diagram was obtained for a constant surfactant content of 2 wt. %. The emulsification failure boundary is sometimes difficult to find, especially for low oil contents, because of long equilibration times.

B. Materials

All samples for the neutron scattering experiments have been prepared in the so-called shell contrast using deuterated water and oil, but hydrogenated surfactant. The nonionic surfactant $C_{10}E_5$ was obtained from Nikko Chemicals Co. Ltd. (Tokyo, Japan). Octane-d_{18} was purchased by Euriso-top Groupe CEA (CE Saclay, Gif-sur-Yvette, France). For this compound the isotopic purity was indicated as 99%. The used D_2O had an isotopic purity of 99.8% and was obtained from the same source. The microemulsions investigated have been freshly prepared before the beginning of the experiments by weighing in the appropriate amounts of the three components. Then the phase transition temperature was determined and the samples were thermostated at a temperature of approximately 1 K above this temperature.

We investigated water continuous microemulsions containing a small dispersed volume fraction ($\phi = 0.043$, composition A). For the DLS experiments we used the hydrogenated compounds, respectively. We prepared samples with $\phi = 0.043$ (composition A). Samples of a somewhat different composition, $\phi = 0.044$ (composition B), were also studied (see Table I). The observed difference in the phase transition

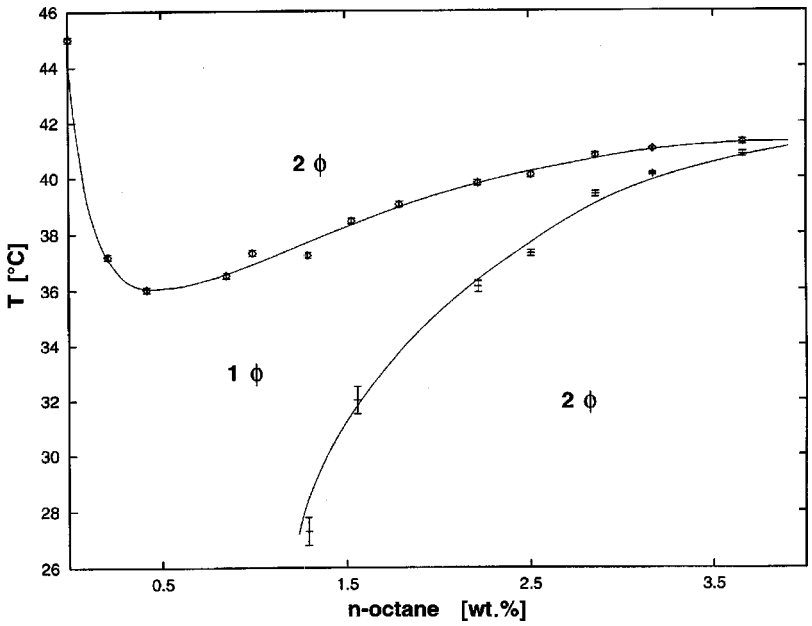

FIG. 1. Phase diagram for C_8H_{18}-$C_{10}E_5$-water mixtures for a constant surfactant content of 2 wt %, which shows the location of the boundaries in the region we investigated. The lower line is the emulsification failure boundary and the upper is the ''haze'' boundary transition to two-phase equilibria. At low temperatures, the microemulsion is in equilibrium with an excess oil phase.

temperature between deuterated and hydrogenated samples is 1.3 K.

C. Experimental setup

1. NSES

The NSES experiments have been performed using the Machine a Echo de Spin de Neutron de Saclay at the Laboratoire Léon Brillouin in Saclay, France (Laboratoire Commune CEA CNRS). Details of the experimental setup can be found elsewhere [35]. Neutrons with a wavelength of 6 Å and a relative linewidth of $\pm$ 18% have been employed in the measurements. The samples were filled into quartz cells of 4 mm thickness. These were positioned in a sample cell holder, which was thermostated at 305.2 K with an accuracy of $\pm$ 0.7 K. The duration of the measurements for one correlation function was between 12 and 16 h. The samples were inspected before and after the measurements and no phase separation was observed.

2. DLS

For the DLS experiments a classical goniometer setup (Amtec, France) and a 72-channel correlator (BI2030-AT, Brookhaven) operated with linear sample time spacing were used. The light source was a krypton ion laser (Innova 90, Coherent) emitting at 647.1 nm, with a constant output power of 400 mW.

Correlation functions were accumulated up to approximately 8×10^5 base line counts to obtain sufficiently good data statistics for a CONTIN analysis of the functions. The samples were first heated to an appropriate temperature well above the phase transition temperature and then filtered into the sample cells through filters with a pore size of 200 nm (Anotop10, Whatman). Before starting the measurements the samples have been thermostated at the desired temperature for at least 2 h. During the measurements at 304 K a small excess oil phase was present.

TABLE I. Sample compositions and parameters.

Sample composition	ϕ_s	ϕ_{oil}	T/(K) $2\Phi\rightarrow1\Phi$
A	0.023	0.02	303.7[a]
B	0.022	0.022	305

[a]Value for the deuterated solvents.

3. SANS

The SANS experiments were carried out at the Laboratoire Léon Brillouin in Saclay using the PAXE instrument. For the measurements the sample was filled into a quartz cell (Hellma) of 2 mm thickness and 1 cm width. The cell was positioned in thermostatable holder and thermostated at the same temperature as for the NSES measurements. The wavelength used was 6 Å. Spectra were recorded at detector distances of 1.5 and 5.05 m covering a total q range 0.008–0.23 $Å^{-1}$. For the detection of the scattering intensity a two-dimensional detector was used. The data at the two detector distances were normalized and corrected for the efficiency of the different detector cells using the spectrum of water [14]. Thereafter, the spectra were radially averaged and finally the data were put on an absolute scale using the method described in Ref. [36].

IV. RESULTS AND DISCUSSION

A. NSES results

For a sample of composition *A* we measured the correlation functions at eight different angles between 2° and 4.5° at a temperature of 305.2$\pm$ 0.7 K. This temperature lies 1.5 K above the phase transition temperature observed for this sample. In Figs. 2 and 3 the different experimentally obtained functions are shown together with their respective single exponential fits. The only adjustable parameter was the effective relaxation rate Γ_{eff} (first cumulant). In Fig. 4 the values obtained for D_{eff} are plotted vs q. A maximum of D_{eff} is observed around $qR\approx\pi$, the first q value at which $f_0(qR)$ vanishes. This is similar to earlier NSES studies on microemulsions [17–19].

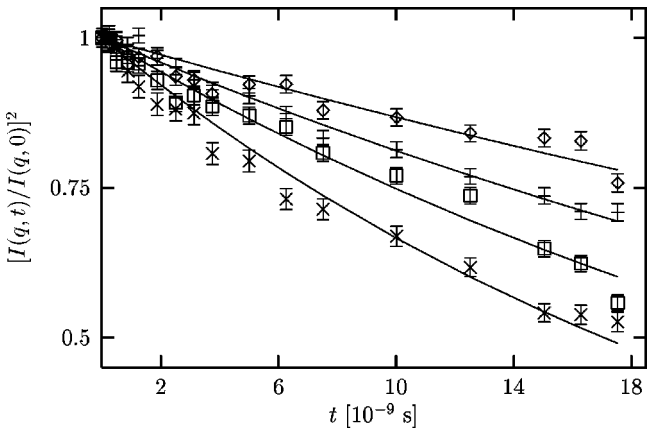

FIG. 2. Fit to spin-echo data using a single exponential function with only one adjustable parameter that corresponds to the first cumulant. Data are for the scattering angles 2° ($\diamond$), 2.5° (+), 2.75° ($\square$), and 3° ($\times$).

B. DLS results

In our DLS experiments we measured samples of compositions A and B. Within the experimental accuracy, the measurements using the different compositions lead to the same results. All samples have been investigated at different scattering angles and temperatures. Correlation functions corresponding to one set of experimental parameters have been measured three times and the values presented in the following are averages over these three measurements.

For the samples with composition B the phase transition towards the single phase region was observed at 305 ± 0.5 K. Therefore, we started the measurements just below this temperature and increased the temperature stepwise to the upper phase boundary, crossing the emulsification failure boundary. In Fig. 5 the values for the translational diffusion coefficients measured at different scattering angles are plotted vs q. Over the q range regarded there are no changes observable and the detected relaxation process is of purely diffusive nature. The correlation functions have been analyzed using CONTIN.

The same behavior is found at 304 K and 306 K. In this temperature range no marked increase in the Stokes radius

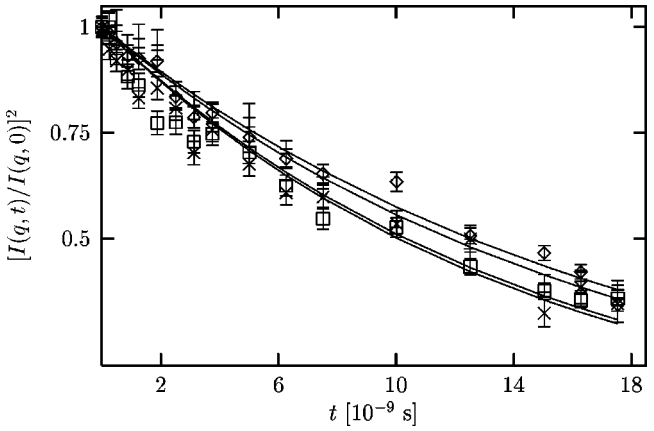

FIG. 3. Fit to spin-echo data using a single exponential function with only one adjustable parameter that corresponds to the first cumulant. Data are for the scattering angles 3° ($\diamond$), 3.5° (+), 4° ($\square$), and 4.5° ($\times$).

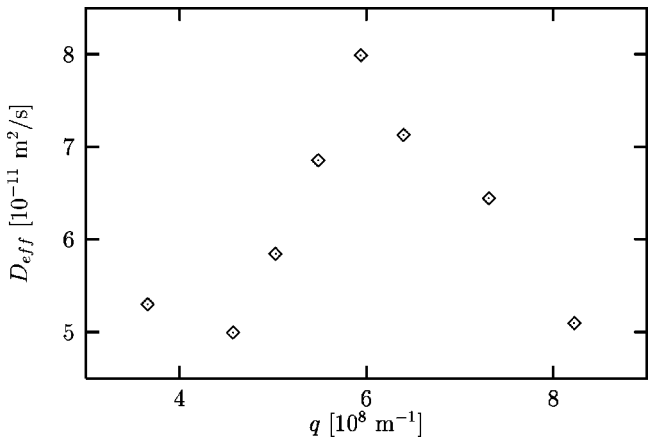

FIG. 4. Effective diffusion coefficients calculated from Γ_{eff} values. The data show the predicted increase of the contribution of the internal modes (mainly the mode with $l=2$) around $qR=\pi$.

obtained is observable. This corresponds to previous results obtained by SANS experiments on similar systems. In those experiments the obtained scattering curves closely below and above the emulsification boundary were indistinguishable [37].

The hydrodynamic radius was calculated from Eq. (26). In view of the experimental accuracy and of the values of k_D for similar systems [30,31], the corrections of Eq. (25) can be neglected. In Fig. 6 these Stokes radii are plotted vs the normalized temperature. In systems where no structural changes occur the radii should be independent of the temperature, as predicted by the Stokes-Einstein equation. For the microemulsions investigated this is clearly not fulfilled. It is interesting that at temperatures up to 2 K above the emulsification failure boundary nearly no changes in the radius occur (within the experimental accuracy of $\pm 5\%$ [38]). At a temperature of 306 K we obtained a hydrodynamic radius of 8.1 ± 0.4 nm.

The hydrodynamic radius becomes large close to the upper two-phase boundary (haze point). These findings correspond to results obtained for the $C_{12}E_5$-water-decane system using nuclear magnetic resonance (NMR) techniques [39,40]

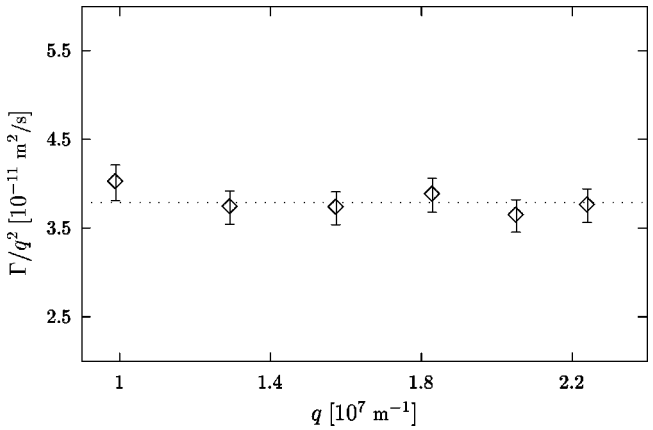

FIG. 5. Plot of the ratio $\overline{\Gamma}/q^2$ vs q. The relaxation mode detected by DLS is purely diffusive. The measurements were made at 305 K. The presented data points represent mean values over three measurements. The dotted line represents the average over all scattering angles.

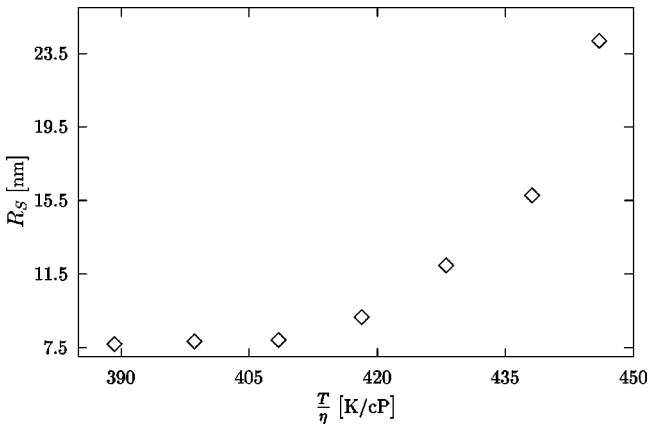

FIG. 6. Plot of the Stokes radii obtained from DLS vs T/η (samples of composition B).

and is supported by recent theoretical works [41]. The best interpretation of the NMR data was obtained assuming a transition from spherical structures to prolate ellipsoids with increasing temperature [40].

For the calculation of the polydispersity using CONTIN, we recursively optimized the frequency window for the transformation, until all grid points lay on the obtained distribution function (in case of monomodal functions). This leads to the best possible description of the relaxation rate distribution. It should be remarked here that this procedure did not change the values obtained for the z average of Γ, but leads to small changes in the higher moments of the distribution. Figure 7 shows some examples for the distribution functions obtained at different scattering angles. The position of the maximum varies as predicted by Eq. (22).

That the size polydispersity of microemulsions can be calculated from DLS data has been shown previously [42,43] using an approach different from that presented here. The values for the polydispersity index p we have computed from our data are listed in Table II. The mean values computed by averaging over all measurements for the respective temperatures are given. The sum of $2\kappa+\overline{\kappa}$ calculated from these p values is slightly smaller than values obtained for the same surfactant-to-oil ratio from SANS (1.81 kT) and interfacial tension measurements (1.6 kT) [44]. The analysis of the correlation functions using a second-order cumulant series was not possible for all the measured functions because some of them were perturbed by contributions of spurious amounts of dust. Therefore, here we discuss only the results obtained employing CONTIN. In the cases where a cumulant fit made sense the obtained polydispersities are significantly lower than the values calculated from the CONTIN results and lie in the range of the value found by the analysis of the SANS data (data from the cumulant fit are not shown). The algorithm used in CONTIN seems to slightly overestimate the polydispersity.

TABLE II. Results from DLS for composition B.

T(K)	p	$2\kappa+\overline{\kappa}$ (units of kT)
304	0.22	1.14
305	0.20	1.27
306	0.20	1.27

C. SANS results

A spectrum taken at $T=305.2$ K is shown in Fig. 8. A calculation of $S(0)$ applying Eq. (29) yields $S(0)=0.68$, which was obtained using an effective hard-sphere volume fraction of $\phi_{hs}=0.049$. As we have addressed in Sec. II D, $S(q)$ becomes 1 for larger q. Therefore, the data have been fitted to the polydisperse shell form factor [13] omitting values below 0.03 Å^{-1}. The intensity for the highest-q value has been subtracted to correct for the incoherent background contribution. The results from the fit are summarized in Table III. For the polydispersity index p the given value is corrected for the instrumental resolution applying $p^2=p_{expt}^2-0.01$ [14,45]. For the radius the fit yields a value of 4.8 ± 0.1 nm (error as obtained from the fitting procedure). For a different sample composition (12.5% less surfactant) Gradzielski and co-workers found a radius of 5.7 nm [44].

The difference between the radius R_0 obtained by SANS and the hydrodynamic radius R_H is surprisingly large. During the experiments no phase separation was observed,

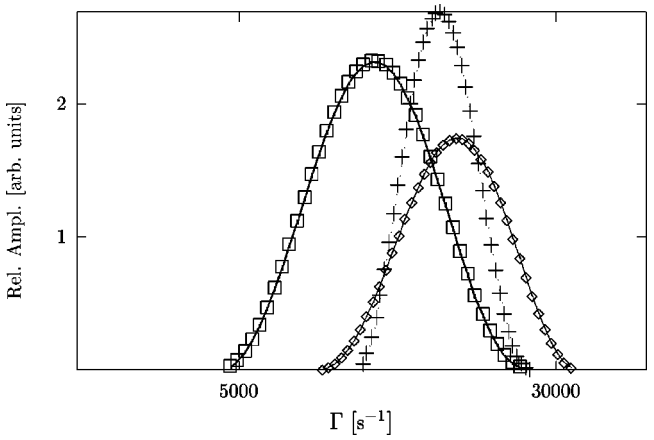

FIG. 7. Three examples of the obtained distribution functions using an optimized frequency window for CONTIN. ◇, $\theta=120°$; +, $\theta=105°$; and □, $\theta=90°$ (samples of composition B).

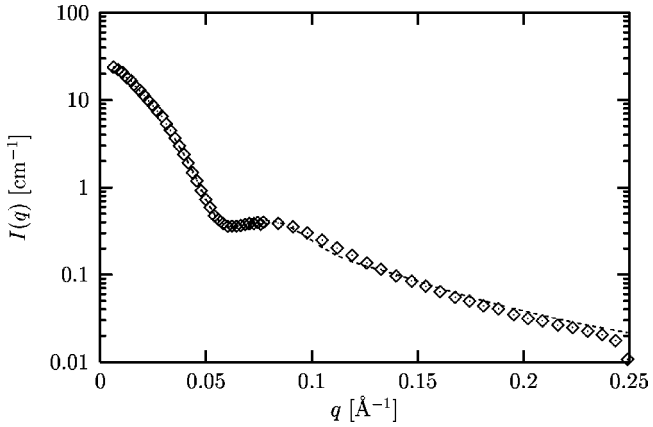

FIG. 8. SANS spectrum for a microemulsion with the same composition as sample A. The dashed line is a fit with the polydisperse shell model. Only values with $q\geq0.03$ Å^{-1} were used in the fit.

TABLE III. Results from SANS.

Sample	R_0 (nm)	t (nm)	T/(K)	p
A	4.8 ± 0.1	0.43	305.9	0.1888

which means that the difference between the two radii cannot be due to the expulsion of oil from the droplets.

If we calculate the length of one surfactant molecule assuming an all transconfiguration we get about 3.3 nm. The fit of the SANS data with the polydisperse shell model gives a value for the radius, which corresponds to the distance between the center of a droplet and the position in the surfactant film where the difference in scattering length density has its maximum.

Because of the curvature of the film and also because of the stronger interaction by means of hydrogen bonds the penetration of D_2O into the film will be stronger than the penetration of the deuterated oil; therefore, it is likely that the radius found by SANS is approximately equivalent to the hydrocarbon radius of the microemulsion droplets. This means that the difference is mainly due to the fact that the large head groups are not ''seen'' by this technique. Considering all this we still have a difference between the two radii that can only be explained assuming four hydration shells.

However, the results that we obtained for another $C_{10}E_5$ based microemulsion containing a different oil (n-dodecane) show the same difference [46]. For the $C_{12}E_5$-decane-water system a hydrodynamic radius of 9.5 nm is reported [30]. SANS data for the same system lead to a radius of 6.8 nm [33]. This compares well with the difference we found for our system.

D. Combined analysis of the results

In the following we will present and discuss the results obtained using a combined fit of DLS and NSES data according to Eq. (14). For the translational diffusion coefficient we took 3.6×10^{-11} m^2/s. This value for the translational diffusion coefficient is obtained from DLS experiments in the temperature region of interest. In Ref. [30] the value of the dynamic virial coefficient k_D for a similar surfactant ($C_{12}E_5$) has been determined [see Eq. (25)]. A correction of the translational diffusion coefficient we determined leads to a change, which lies within the experimental error interval (5%).

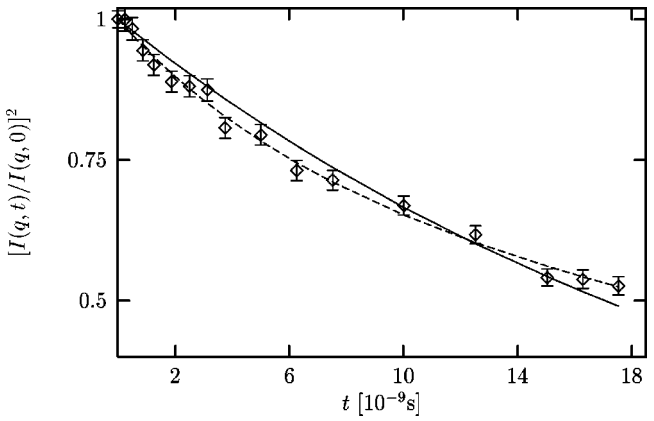

FIG. 9. Fit using a double exponential with two adjustable parameters (dashed line) in comparison to the single exponential fit (solid line).

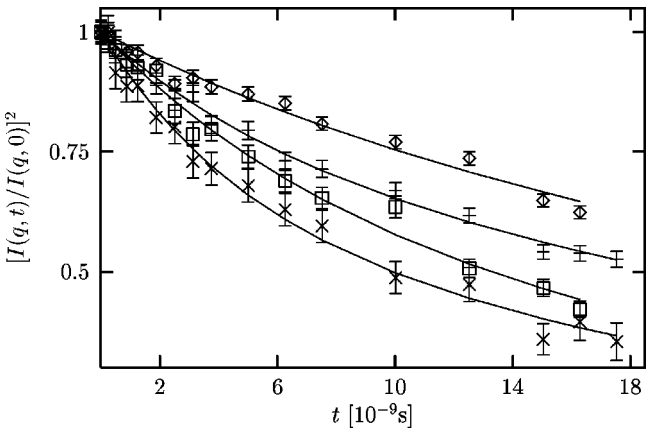

FIG. 10. Fit using a double exponential with two adjustable parameters. Data are shown for the scattering angles 275° ($\diamond$), 3° (+), 3.25° ($\square$), and 3.5° ($\times$). The functions shown have been squared before fitting with the square of Eq. (14).

In Fig. 9 the double exponential fit to Eq. (14) is shown in comparison to a simple two parameter single exponential fit. The representation of the data is much better without increasing the number of adjustable parameters. In Fig. 10 the double exponential fits for some of the measured angles are shown. From the relaxation rate of the second exponential in Eq. (14) it is now possible to calculate τ_2. In Fig. 11 the relaxation rates obtained for the different scattering angles are plotted. A slight q dependence is still observable. Especially, at higher q the contribution of the modes corresponding to $l>2$ seems to increase remarkably. At scattering angles of 2° and 2.5° it is not possible to extract a reliable value for τ_2 because the contribution (the amplitude) of the shape fluctuations is too low.

In Fig. 12 the amplitudes of the second exponential extracted from the fit parameter a are shown. The second contribution to the measured NSES relaxation curves has a maximum where also in Fig. 4 the maximum is observed. The maximum occurs at $qR\approx3$.

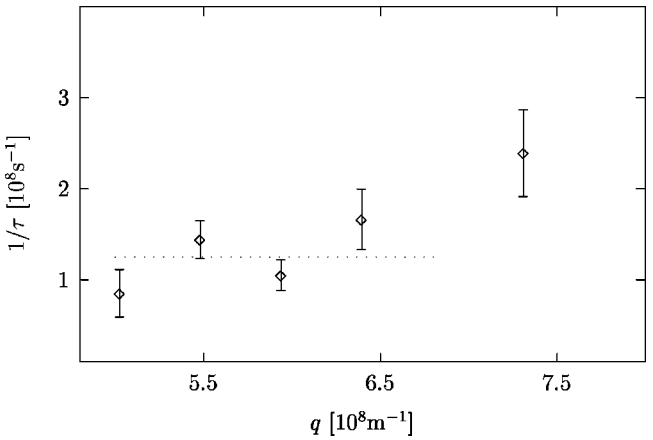

FIG. 11. Relaxation rates τ_2^{-1} obtained using the double exponential fit according to Eq. (14). At higher q the relaxation rates still show a slight increase because of the increasing contributions of modes corresponding to $l>2$.

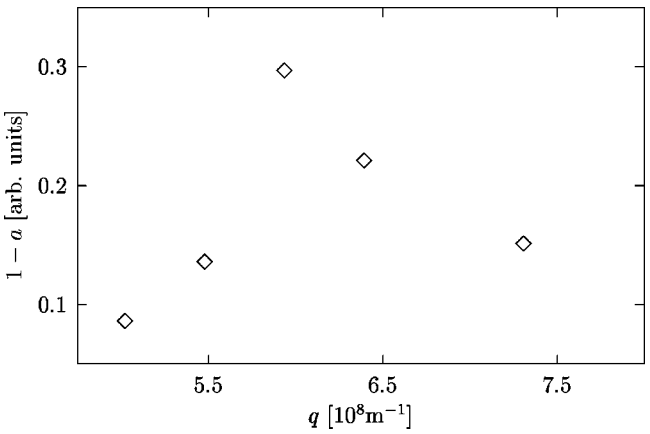

FIG. 12. Plot of the amplitudes $1-a$ of the second exponential vs q. The amplitudes show the same behavior as the values of D_{eff} in Fig. 4. The amplitudes show qualitatively the behavior predicted by Eq. (17), but the absolute values differ from the right-hand side of Eq. (17).

In the low-q limit the relaxation rates obtained do not show a significant dependence on q (indicated by the dotted line in Fig. 11). Therefore, it seems to be straightforward to calculate a mean relaxation time for the $l=2$ modes from these values. We find a value of 8.3 ns for τ_2. The error bars of the relaxation times in Fig. 11 represent an error of approximately 10% and are obtained from the fitting procedure.

Equation (5) now allows one to compute the sum $4\kappa-\bar{\kappa}$ from this value. In our calculations we used Eq. (7) to account for the unequal viscosities. For the radius we used the value obtained from the SANS experiments because this value should be a good representation for the curvature of the so-called neutral surface. The employed viscosities are 0.4675 cP (*n*-octane) and 0.7632 (water). With these values we get $4\kappa-\bar{\kappa}=4.05$ kT. Using the value for $2\kappa+\bar{\kappa}$ obtained from the polydispersity index, it is now possible to calculate the two elastic constants. With the polydispersity index obtained from our SANS experiments we finally end up with $\kappa=0.92$ kT and $\bar{\kappa}=-0.38$ kT. Using the polydispersity index calculated from the DLS correlation functions leads to $\kappa=0.88$ kT and $\bar{\kappa}=-0.52$ kT, respectively.

These values are in good agreement with results obtained by other techniques for similar systems and the values obtained for $\bar{\kappa}$ agree with theoretical predictions for droplet phases [21]. Sottmann and Strey recently published values of the bending elastic constants for the system we investigated here. They found 0.9 kT for κ and -0.31 kT for $\bar{\kappa}$ using the spinning-drop method [47]. For the relative error of the elastic constants 25% should be a good estimate.

In previous NSES studies of microemulsions the values obtained for κ were much higher and did not correspond to results from other experiments. For the surfactant $C_{12}E_5$, for example, a value of 4 kT is reported [19].

V. CONCLUSIONS

We presented an alternative approach to the analysis of NSES data measured for droplet microemulsions using a combined fit of NSES and DLS data. This method allows for a direct determination of the relaxation times of the mode corresponding to the spherical harmonic with $l=2$.

Moreover, this method allows for a calculation of the bending elastic constants if the size polydispersity of the microemulsion droplets is known. The values of the bending elastic constants obtained by this approach correspond much better to results derived from other experiments than in previous NSES studies. In the future it has to be further clarified which radius gives the best description of the curvature of the microemulsion droplets and therefore has to be employed in the calculation of $4\kappa-\bar{\kappa}$.

The experimental techniques of NSES and DLS in combination are an excellent tool for the study of the dynamics in microemulsions because both techniques measure the same dynamics but in different time domains. Approaches similar to those presented here should also be useful in the study of polymer dynamics.

ACKNOWLEDGMENTS

This project was supported by a grant of EC (Grant No. ERB4050PL920671). We are grateful to A. Brulet and O. Choquet for help with the NSES experiments and to L. T. Lee for help with the PAXE spectrometer. We would like to thank S. Safran, Th. Sottmann, M. Gradzielski, and R. Strey for fruitful discussions. The neutron scattering experiments were carried out at the Laboratoire Léon Brillouin, Laboratoire Commun de CEA, CNRS.

[1] P. G. de Gennes and C. Taupin, J. Phys. Chem. **86**, 2294 (1982).
[2] D. Langevin, Annu. Rev. Phys. Chem. **43**, 341 (1992).
[3] L. E. Scriven, Nature (London) **263**, 123 (1976).
[4] W. Helfrich, Z. Naturforsch. C **28**, 693 (1973).
[5] S. T. Milner and S. A. Safran, Phys. Rev. A **36**, 4371 (1987).
[6] M. Borkovec, J. Chem. Phys. **91**, 6268 (1989).
[7] S. A. Safran and L. A. Turkevich, Phys. Rev. Lett. **50**, 1930 (1983).
[8] L. T. Lee, D. Langevin, and R. Strey, Physica A **168**, 210 (1990).
[9] E. van der Linden, S. Geiger, and D. Bedeaux, Physica A **156**, 130 (1989).
[10] M. Borkovec and H.-F. Eicke, Chem. Phys. Lett. **157**, 457 (1989).
[11] B. P. Binks, J. Meunier, O. Abillon, and D. Langevin, Langmuir **5**, 415 (1989).
[12] H. Kellay, J. Meunier, and B. P. Binks, Phys. Rev. Lett. **70**, 1485 (1993).
[13] M. Gradzielski, D. Langevin, L. Magid, and R. Strey, J. Phys. Chem. **99**, 13 232 (1995).
[14] M. Gradzielski, D. Langevin, and B. Farago, Phys. Rev. E **53**, 3900 (1996).
[15] M. Kahlweit and R. Strey, Angew. Chem. **97**, 655 (1985).
[16] R. Strey, Colloid Polym. Sci. **272**, 1005 (1994).

[17] J. S. Huang, S. T. Milner, B. Farago, and D. Richter, Phys. Rev. Lett. **59**, 2600 (1987).
[18] B. Farago, D. Richter, J. S. Huang, S. A. Safran, and S. T. Milner, Phys. Rev. Lett. **65**, 3348 (1990).
[19] B. Farago, M. Monkenbusch, K. D. Goecking, D. Richter, and J. S. Huang, Physica B **213**, 712 (1995).
[20] S. A. Safran, J. Chem. Phys. **78**, 2073 (1983).
[21] S. A. Safran, Phys. Rev. A **43**, 2903 (1991).
[22] S. Komura and K. Seki, Physica A **192**, 27 (1993).
[23] *Neutron Spin Echo*, edited by F. Mezei, Lecture Notes in Physics Vol. 129 (Springer-Verlag, Berlin, 1980).
[24] R. J. Papoular and A. K. Livesey, in *Maximum Entropy and Bayesian Methods*, edited by J. Skilling (Kluwer Academic, Dordrecht, 1989), pp. 163–173.
[25] D. E. Koppel, J. Chem. Phys. **57**, 4814 (1972).
[26] S. S. Sorlie and R. Pecora, Macromolecules **21**, 1437 (1988).
[27] B. J. Berne and R. Pecora, *Dynamic Light Scattering* (Wiley, New York, 1976).
[28] S. W. Provencher, Comput. Phys. Commun. **27**, 213 (1982).
[29] S. W. Provencher, Comput. Phys. Commun. **27**, 229 (1982).
[30] U. Olsson and P. Schurtenberger, Langmuir **9**, 3389 (1993).
[31] M. Gradzielski and H. Hoffmann, J. Phys. Chem. **98**, 2613 (1994).
[32] Carl Robertus, Ph.D. thesis, Rijksuniversiteit Utrecht, 1990 (unpublished).
[33] H. Bagger-Jörgensen, U. Olsson, and K. Mortensen, Langmuir **13**, 1413 (1997).
[34] N. F. Carnahan and K. E. Starlin, J. Chem. Phys. **51**, 635 (1969).
[35] R. Papoular, Ph.D. thesis, Université de Paris–Sud, 1992 (unpublished).
[36] J. P. Cotton, in *Neutron, X-Ray and Light Scattering*, edited by P. Lindner and Th. Zemb (Elsevier Science, Amsterdam, 1991).
[37] F. Sicoli and D. Langevin, J. Phys. Chem. **99**, 14 819 (1995).
[38] Th. Hellweg, *Makromolekulare Strukturen in Einem Anderen Licht* (Cuvillier, Göttingen, 1996).
[39] M. S. Leaver, U. Olsson, H. Wennerström, and R. Strey, J. Phys. II **4**, 515 (1994).
[40] M. Leaver, I. Furó, and U. Olsson, Langmuir **11**, 1524 (1995).
[41] T. Tlusty, S. A. Safran, R. Menes, and R. Strey, Phys. Rev. Lett. **78**, 2616 (1997)
[42] M. Kotlarchyk, R. B. Stephens, and J. S. Huang, J. Phys. Chem. **92**, 1533 (1988).
[43] J. Ricka, M. Borkovec, and U. Hofmeier, J. Chem. Phys. **94**, 8503 (1991).
[44] M. Gradzielski, D. Langevin, T. Scottmann, and R. Strey, J. Chem. Phys. **106**, 8232 (1997).
[45] F. Sicoli, D. Langevin, and L. T. Lee, J. Chem. Phys. **99**, 4759 (1993).
[46] Th. Hellweg and D. Langevin (unpublished).
[47] T. Sottmann and R. Strey, J. Chem. Phys. **106**, 8606 (1997).